Research Square

Preprints are preliminary reports that have not undergone peer review.
They should not be considered conclusive, used to inform clinical practice,
or referenced by the media as validated information.

Multi-parameter and multi-layer observations of precursors to the 2026 Kumamoto earthquake (Mj=7.1)

Masashi Hayakawa
QuakeInsight Tokyo, UEC Alliance Center
Hide'aki Hinata
QuakeInsight Tokyo, UEC Alliance Center
Shinji Hirooka
HiSR Inc., 2-2-15 Minami-Aoyama, Minato-ku
Shih-Sian Yang
Chang Jung Christian University
Yasuhide Hobara
University of Electro-Communications
Kousik Nanda
Institute of Astrnomy Space and Earth Science
Stelios M Potirakis
University of West Attica Aigaleo Grove Campus: Panepistemio Dytikes Attikes Panepistemioupole Alsous Aigaleo https://orcid.org/0000-0001-5928-4587
Sudipta Sasmal
meet2ss25@gmail.com

Institute of Astronomy Space and Earth Science

Research Article

Keywords:

Posted Date: November 19th, 2026

DOI: https://doi.org/10.21203/rs.3.rs-11373711/v1

License: This work is licensed under a Creative Commons Attribution 4.0 International License.
Read Full License

Multi-parameter and multi-layer observations of precursors to the 2026 Kumamoto earthquake (Mj=7.1)

Masashi Hayakawa[1,2,3], Hide'aki Hinata[3], Shinji Hirooka[4,3], Shih-Sian Yang[5,3], Yasuhide Hobara[1,6], Kousik Nanda[7,8], Stelios M. Potirakis[9,10,3], Sudipta Sasmal[7,3*]

[1]Department of Computer and Network Engineering, The University of Electro-Communications (UEC), 1-5-1 Chofugaoka, Chofu, 182-8585, Japan.

[2]Advanced Wireless & Communications Research Center (AWCC), The University of Electro-Communications (UEC), 1-5-1 Chofugaoka, Chofu, 182-8585, Japan.

[3]QuakeInsight Tokyo, UEC Alliance Center #501, 1-1-1 Kojima-cho, Chofu, 182-0026, Japan.

[4]HiSR Inc., 2-2-15 Minami-Aoyama, Minato-ku, Tokyo, 107-0062, Japan.

[5]Environmental Research and Information Center, Chang Jung Christian University, No. 1 Changda Road, Gueiren, Tainan, 711301, Taiwan.

[6]Center for Space Science and Radio Engineering, The University of Electro-Communications (UEC), 1-5-1 Chofugaoka, Chofu, 182-8585, Japan.

[7]Institute of Astronomy Space and Earth Science, P 177, CIT Road, Scheme 7M, Kolkata, 700054, India.

[8]Department of Computer Science and Application, Prabhat Kumar College, Contai, India.

[9]Department of Electrical and Electronics Engineering, University of West Attica, Ancient Olive Grove Campus, Egaleo, Greece.

[10]Institute for Astronomy, Astrophysics, Space Applications and Remote Sensing, National Observatory of Athens, Metaxa and Vasileos Pavlou, Athens, Greece.

*Corresponding author(s). E-mail(s): sudipta@iases.org.in;

Contributing authors: hayakawa@quakeinsight.tokyo;
hinata@quakeinsight.tokyo; hirooka@hrl.jp; yang.sirius.sian@gmail.com;
hobara@ee.uec.ac.jp; kncontai@gmail.com; spoti@uniwa.gr;

Abstract

This paper summarizes multi-parameter and multi-layer observations associated with the recent large Kumamoto earthquake (EQ) ($\boldsymbol{M_j = 7.1}$), which occurred on 28 July 2026 at geographic coordinates **32.61**°N, **130.67**°E. After examining the solar–terrestrial conditions, we demonstrate several possible precursory signatures associated with this EQ, with particular emphasis on ground-based observations because of their comparatively high temporal and spatial resolutions. First, we examine meteorological parameters, including temperature ($\boldsymbol{T}$), relative humidity (RH), and atmospheric chemical potential (ACP). Among these parameters, the more stable quantity, ACP, appears to increase beginning on 22 July, six days before the EQ, and this enhancement persists through the day of the EQ and even into the post-EQ period. Using ACP values observed at various stations at 00:00 JST on 23 July, when the midnight enhancement was evident, we construct a spatial contour map of ACP, and the maximum ACP enhancement is found to be located very close to the EQ epicenter in the Hinagu fault region. We then investigate lower-ionospheric perturbations using propagation anomalies along the paths from the VLF transmitter JJI, located at Ebino, Miyazaki Prefecture, to two VLF receiving stations located in Osaka and Chofu. The nighttime signal amplitude begins to exhibit anomalous behavior on 23 July, approximately five days before the EQ, and one day before the EQ, a conspicuous depletion below $\boldsymbol{-2.0\sigma}$ ($\boldsymbol{\sigma}$ denotes the standard deviation) is observed at Osaka. The corresponding VLF observations at Chofu show an anomaly on the same day, although with a smaller depletion, providing additional support for the perturbation detected along the JJI–Osaka propagation path. Finally, we examine F-region ionospheric anomalies using vertical ionospheric sounding observations at Yamagawa, located close to the EQ epicenter. By comparing the Yamagawa observations with those from three other Japanese ionosonde stations, we identify oscillatory variations occurring only at Yamagawa from 12:00 JST on 26 July to 12:00 JST on 27 July, corresponding to approximately 1.2–2.2 days before the EQ, and these oscillatory signatures are further examined using wavelet analysis. The ground-based observations are supplemented by satellite-based measurements of $\boldsymbol{T}$, RH, ACP, GPS total electron content (TEC), ERA-based atmospheric gravity wave (AGW) activity, and mesosphere/thermosphere parameters derived from the TIMED/SABER satellite. In particular, the satellite-derived $\boldsymbol{T}$, RH, and ACP parameters provide additional support for the corresponding ground-based results. Overall, the satellite observations indicate a distinct clustering of pre-EQ thermal and ionospheric anomalies approximately two days before the earthquake, followed by stronger acoustic and mesospheric variability around and after the event. The precursory effects detected in the different atmospheric and ionospheric layers occur within a relatively narrow temporal interval, and ionospheric perturbations detected by sub-ionospheric VLF observations, together with several other possible precursory signatures, occur in close association with perturbations observed near the Earth's surface. These results suggest that the 2026 Kumamoto earthquake may

represent a case of the fast channel of direct lithosphere–atmosphere–ionosphere coupling (LAIC).

Keywords: The 2026 Kumamoto earthquake (EQ), AMeDAS meteorological parameters, ACP (atmospheric chemical potential), sub-ionospheric VLF propagation, ionosonde observation, satellite observations, GPS TEC (total electron content), mesosphere/thermosphere parameters, lithosphere-atmosphere-ionosphere coupling (LAIC)

1 Introduction

Disasters caused by major to strong earthquakes (EQs) are very serious and can cause significant damage to societies, economies, and environments. Therefore, conducting short-term precursory research for EQs, with a lead time of approximately one week, has long been a major challenge in geophysics. Enormous progress has been achieved, particularly in studies of EQ precursors in different geo-layers, including the lithosphere, atmosphere, and ionosphere, despite the complexity of the EQ nucleation process and the difficulty of distinguishing pre-seismic anomalies from the background of diverse natural variability in the lithosphere, atmosphere, and ionosphere (Pulinets and Boyarchuk 2004; Molchanov and Hayakawa 2008; Hayakawa 2009; Sorokin et al. 2015; Hayakawa 2015; Ouzounov et al. 2018; Pulinets et al. 2020; Conti et al. 2021; Picozza et al. 2021; Sasmal et al. 2021; Blaunstein and Hayakawa 2026).

Researchers have identified different EQ precursors in various geo-layers, such as the lithosphere, atmosphere, and ionosphere, and have found them to be statistically correlated with seismicity Liu et al. (2013); Parrot and Li (2018); Hayakawa (2025). These layers are considered to be strongly coupled through complex mechanisms, leading to the concept of lithosphere–atmosphere–ionosphere coupling (LAIC) Molchanov et al. (2004); Hayakawa (2004); Pulinets and Ouzounov (2011). Extensive multi-parameter studies have been conducted over the past decade for various strong EQ events worldwide to improve our understanding of the LAIC process Akhoondzadeh et al. (2019); De Santis et al. (2020); Marchetti et al. (2020); Draz et al. (2023); Zhang et al. (2023); Ouzounov et al. (2021); Parrot et al. (2021); Sasmal et al. (2021); Hayakawa et al. (2021, 2022); D'Arcangelo et al. (2023); Liu et al. (2023); Shah et al. (2023); Marchetti et al. (2024a,b); Haider et al. (2024); Hayakawa and Hobara (2024); Sasmal et al. (2024, 2025). However, the LAIC process is still not fully understood, although several hypotheses have been proposed to explain the underlying coupling mechanisms Molchanov et al. (2004).

As a consequence of the scientific progress in LAIC studies, we are now approaching the practical stage of short-term EQ prediction De Santis et al. (2025), based on multi-parameter and multi-layer observations, because predicting an EQ using only a single parameter is highly questionable Sasmal et al. (2021); Hayakawa et al. (2021); De Santis et al. (2020); Hayakawa (2025); Hayakawa and Hobara (2024). Most of the studies cited above have investigated the LAIC process primarily using satellite observations of in situ physical parameters, such as electron density and magnetic field,

together with satellite monitoring of Earth's surface and lower-atmospheric parameters, including meteorological quantities such as temperature (T) and relative humidity (RH). Consequently, there has been a substantial lack of observational information concerning the intermediate region between satellite altitudes of approximately 500–600 km and the Earth's surface. Only a limited number of studies have focused extensively on this intermediate region, particularly the lower ionosphere investigated using sub-ionospheric VLF/LF propagation Rodger and Cliverd (1999); Molchanov and Hayakawa (2008); Hayakawa (2015, 2025); Sasmal et al. (2021); Politis et al. (2024); Nanda et al. (2026). These studies have emphasized the essential importance of observations in this region both for the scientific elucidation of the LAIC process and for the practical implementation of short-term EQ prediction.

We should also mention that our new affiliation, QuakeInsight Tokyo (QIT Tokyo), established in 2025, was created as a dedicated platform to advance the practical development of short-term EQ prediction for major to strong EQs in the Kanto (Tokyo) region through coordinated multi-parameter observations. QIT Tokyo is currently constructing and expanding its observational networks, developing standardized analysis algorithms, and integrating individual observational parameters into an automated monitoring framework. The initial core parameters include: (1) meteorological anomalies derived from the Japan Meteorological Agency (JMA) open-access Automated Meteorological Data Acquisition System (AMeDAS) network, with particular emphasis on variations in temperature/relative humidity (T/RH) and atmospheric chemical potential (ACP); (2) lower-ionospheric perturbations monitored using sub-ionospheric VLF/LF transmitter signals from two Japanese transmitters, JJY (40 kHz, Fukushima; geographic coordinates: 37.37°N, 140.84°E) and JJI (22.2 kHz, Ebino, Miyazaki Prefecture; 32.08°N, 130.82°E), together with two overseas transmitters, NWC (19.8 kHz, Australia; 21.82°S, 114.17°E) and NPM (21.4 kHz, Hawaii; 21.42°N, 158.15°W), observed at Chofu (35.65°N, 139.54°E) and Osaka (34.84°N, 135.41°E); and (3) F-region ionospheric electron density, particularly $N_{\mathrm{m}}F_2$, observed by the National Institute of Information and Communications Technology (NICT) at Kokubunji, Tokyo. Analysis algorithms for these three principal observational components have already been developed. A particularly important role of QIT Tokyo is to provide a common operational platform in which these heterogeneous parameters are integrated into an automated processing chain consisting of automated data acquisition and transmission, automated analysis toolkits, synchronized anomaly evaluation, and unified visualization using a dashboard-type monitoring system. This framework enables the simultaneous examination of different atmospheric and ionospheric observations and provides a basis for rapid application to recent significant EQ events, including the 2026 Kumamoto EQ, in order to investigate possible precursory electromagnetic phenomena and the associated LAIC processes.

The ground-based observations are further complemented by a range of spaceborne and reanalysis-based measurements to examine vertical coupling throughout the atmosphere and ionosphere. These supplementary datasets include T, RH, and ACP-related atmospheric parameters; GPS-derived total electron content (GPS-TEC); atmospheric gravity wave (AGW) activity investigated using ERA reanalysis data; and additional middle- and upper-atmospheric parameters from the TIMED satellite,

including measurements relevant to the mesosphere and thermosphere. By combining these observations with the QIT ground-based monitoring network, this study aims to construct a more comprehensive picture of the temporal and spatial evolution of possible EQ-related anomalies from the lower atmosphere through the ionosphere. The final objective is to synthesize the results from all observational channels and discuss the most plausible LAIC coupling processes or pathways based on their overall consistency, timing, altitude dependence, and mutual correspondence.

2 The 2026 Kumamoto EQ

On 28 July 2026 at 16:27 JST (07:27 UT), a major earthquake (EQ) occurred in Kumamoto Prefecture on the southern Japanese island of Kyushu, with an epicentral location of 32.682°N, 130.722°E. The Japan Meteorological Agency (JMA) determined a magnitude of $M_j = 7.1$, whereas the United States Geological Survey (USGS) reported a moment magnitude of $M_w = 6.8$. Based on the empirical relation proposed by Dobrovolsky et al. (1979), the estimated EQ preparation zone extends to a radius of approximately 840 km. Figure 1 shows the epicenter of the 2026 Kumamoto EQ (large red circle) and the major regional fault systems. The EQ involved strike-slip faulting and likely occurred along the southern segment of the Hinagu Fault, shown by the green lines in Figure 1, which forms part of the broader Beppu–Haneyama Fault Zone. The same tectonically active region was affected by the destructive 2016 Kumamoto EQ sequence, primarily associated with the Futagawa Fault system (blue lines in Figure 1), which resulted in 273 fatalities and extensive regional damage. The epicenter of the 2026 event was located near the coastal city of Uto, approximately 20 km south of Kumamoto City. The EQ occurred at a shallow focal depth of about 16 km, resulting in very strong ground motion across the affected region. The maximum observed seismic intensity reached JMA intensity 7 in Uki City and Hikawa Town. The event caused 39 fatalities, several hundred injuries, and widespread structural damage. Owing to its shallow focal depth, large magnitude, and occurrence within a well-developed active fault system, the 2026 Kumamoto EQ provides an important case for investigating possible pre-seismic atmospheric and ionospheric anomalies and their relationship to lithosphere–atmosphere–ionosphere coupling (LAIC) processes.

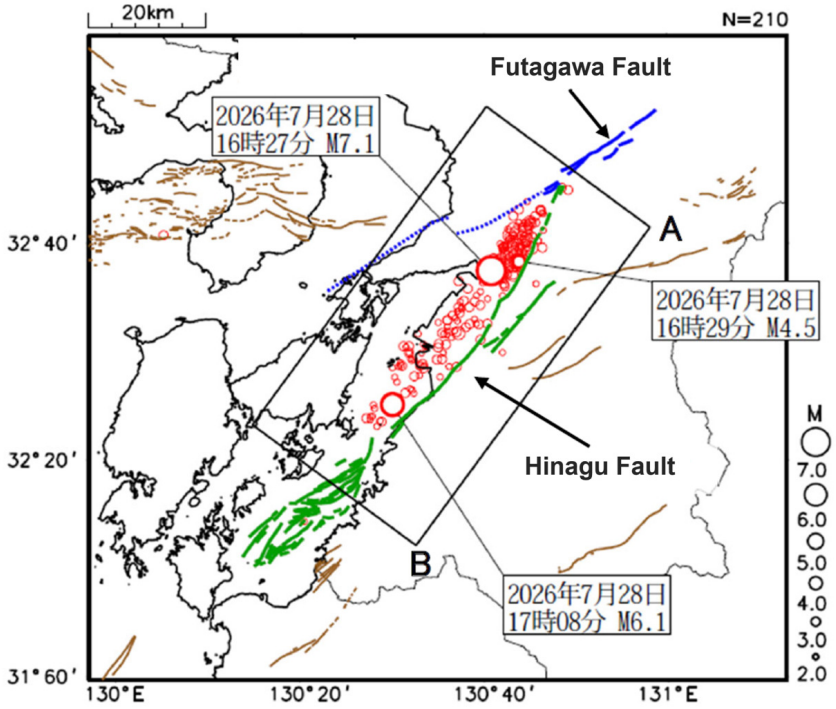


Fig. 1: Location of the epicenter of the main shock of the 2026 Kumamoto earthquake (EQ) (upper largest circle) and the spatial distribution of its aftershocks during the period from 16:00 to 19:00 JST on 28 July 2026. Two major fault regions are also indicated: the Hinagu Fault, considered responsible for the present Kumamoto EQ and shown by green lines, and the Futagawa Fault, shown by blue lines, which was associated with the 2016 Kumamoto EQ. Adapted from the JMA Report (2026).

3 Solar-terrestrial conditions

When investigating possible seismogenic precursors associated with an earthquake (EQ), it is essential to examine the prevailing solar–terrestrial, or space-weather, conditions in detail, since externally driven geomagnetic and ionospheric disturbances may obscure or mimic signals of possible seismic origin. Figure 2 presents the temporal evolution of the principal solar–terrestrial parameters during the period preceding and following the EQ, including the Dst index (nT), Kp index, Ap index, solar radio flux at 10.7 cm (F10.7), and the interplanetary magnetic field (IMF). The geomagnetic environment exhibited appreciable variability throughout the analysis interval. The most pronounced pre-EQ geomagnetic activity occurred five days before the event, on DOY 204, when the mean Kp index reached approximately 5.7, the 3-hourly Ap index peaked at 65, and the daily Ap index reached 28, indicating enhanced geomagnetic activity. During the earlier part of the interval, particularly between DOY 196

and 202, Ap decreased to values as low as 0, while the F10.7 index varied approximately between 100 and 160, reflecting changes in solar activity. However, because complete geomagnetic parameter values are not available for each of the final one to two days immediately preceding the EQ, no definitive quiet or disturbed classification is assigned to those specific near-event intervals. This screening identifies periods potentially influenced by solar–terrestrial forcing and avoids attributing externally driven ionospheric disturbances to seismogenic processes without sufficient supporting evidence.

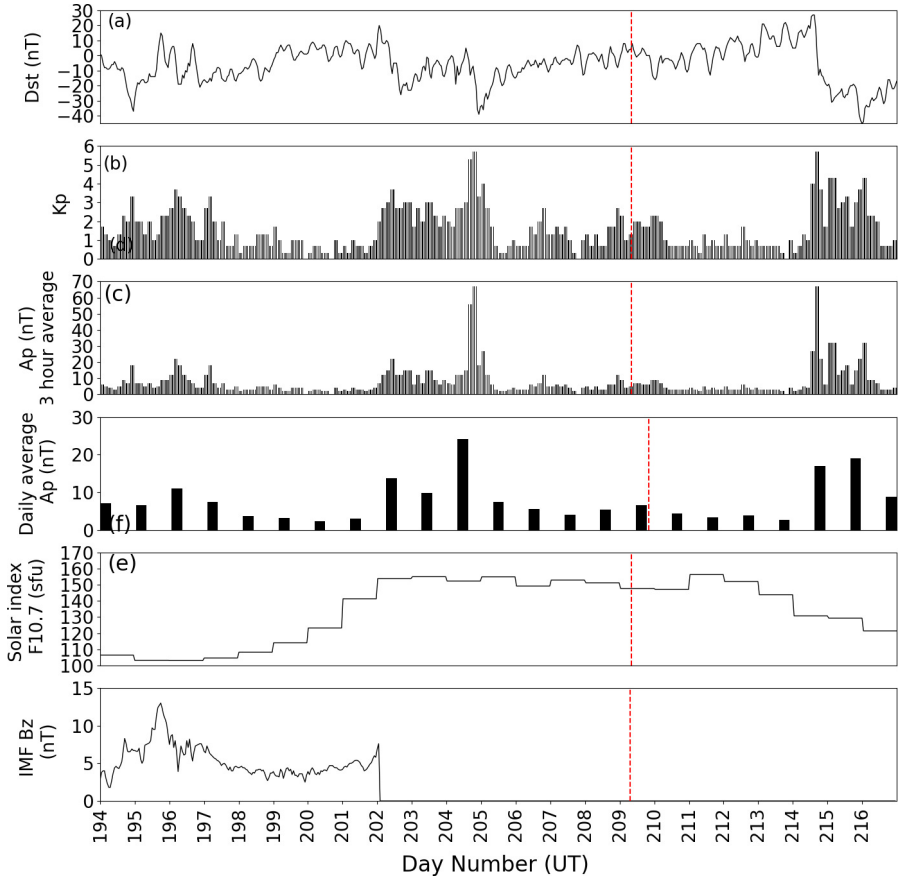


Fig. 2: Temporal evolution of solar–terrestrial conditions before and after the occurrence of the EQ. The panels show geomagnetic activity represented by the Dst, Kp, and Ap indices, solar activity expressed by the F10.7 solar radio flux, and the interplanetary magnetic field (IMF). The vertical red line indicates the EQ occurrence time.

4 Methodology and Observational Results

4.1 Methodology

A multi-parameter analysis was performed to assess lithosphere–atmosphere–ionosphere perturbations associated with the EQ. Near-surface thermodynamic variability was investigated using NOAA reanalysis air temperature and relative humidity data to derive the atmospheric chemical potential (ACP), and daily mean regional fields were constructed to identify thermal and humidity anomalies and examine their temporal and spatial evolution. Middle-atmospheric responses were investigated using ERA5 temperature profiles, with gravity-wave-scale perturbations isolated through digital filtering techniques and atmospheric stability evaluated using parameters such as the Brunt–Väisälä frequency and gravity-wave potential energy, particularly in the upper stratosphere–lower mesosphere region where wave amplitudes generally increase with altitude. Ionospheric disturbances were examined using very-low-frequency (VLF) nighttime fluctuation indices, with anomalies identified as deviations exceeding the $\pm 2\sigma$ limits calculated from a 31-day reference period. Simultaneously, total electron content (TEC) was derived from dual-frequency GPS observations and converted into vertical TEC (VTEC), while anomalous variations were identified using median and interquartile-range (IQR) statistics and their regional spatial distributions were further assessed using JPL GUARDIAN TEC maps. Mesospheric and lower-thermospheric variability was examined using temperature and related atmospheric profiles obtained from the TIMED/SABER instrument to characterize altitude-dependent thermal perturbations and possible wave signatures associated with vertical atmospheric coupling. Overall, this integrated multi-parameter approach provides a comprehensive framework for investigating possible perturbations extending from the near-surface atmosphere through the middle and upper atmosphere to the ionosphere in association with the EQ.

4.2 Meteorological Anomalies

Pioneering work Tronin (2002); Tronin et al. (2002) on NOAA satellite observations of Earth's surface thermal anomalies suggested positive thermal anomalies associated with impending EQs in Japan and China, including the 1995 Kobe EQ. Their findings are, (a) thermal anomalies (up to 4–5 °C) are sensitive to crustal EQs, appearing 7–10 days before an EQ. Since these works, there have been published too many papers on satellite observations of Earth's surface meteorological parameters (such as T, RH, etc.) and associated lower atmospheric physical parameters like SLHF (surface latent heat flux), OLR (outgoing longwave radiation), etc., to cite (see, e.g., Hayakawa et al. (2025); Ghosh et al. (2024); Hinata et al. (2025); Hayakawa et al. (2025), and many references therein).

Recently, the importance of the two physical parameters of T/RH and ACP has been emphasized Hayakawa et al. (2025), with ACP initially proposed in Pulinets and Boyarchuk (2004), using open-access meteorological data (so-called AMeDAS (automatic meteorological data acquisition system) data) provided by JMA (Japan Meteorological Agency). Our QIT has already developed continuous monitoring of

these two parameters in and around Tokyo District, but it can be readily applied to Kyushu Island.

Figure 3(a) illustrates the temporal evolution of ACP (in eV) at a particular AMeDAS station of Kumamoto as one of the stations closest to the EQ epicenter among about 70 stations in Kyushu. We have applied exactly the same residual analysis as in VLF analysis in the next subsection (σ), to the meteorological parameters, and the values are normalized by its standard deviation. The vertical red line indicates the time of occurrence of the Kumamoto EQ. Though not shown, another parameter of T/RH is found to exhibit quite similar temporal evolutions to those of ACP, so we have plotted only the parameter of ACP, because it is recognized to be very stable at night Hinata et al. (2025). The value of ACP seems to be enhanced starting from 20 July, eight days before the EQ, and this enhancement lasts until the occurrence of the EQ and even after the EQ. These meteorological anomalies can probably be explained by the emanation of radioactive radon gases and the associated physico-chemical consequences Hinata et al. (2025).

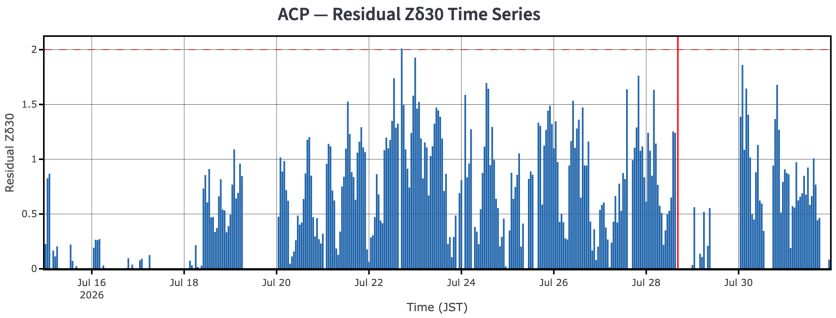


Figure 3(a). Temporal evolution of the residual ACP values before and after the EQ occurrence. The residual values are normalized by their standard deviation (σ), and only ACP values above the mean are plotted; values below the mean are not shown. The red vertical line indicates the EQ occurrence time.

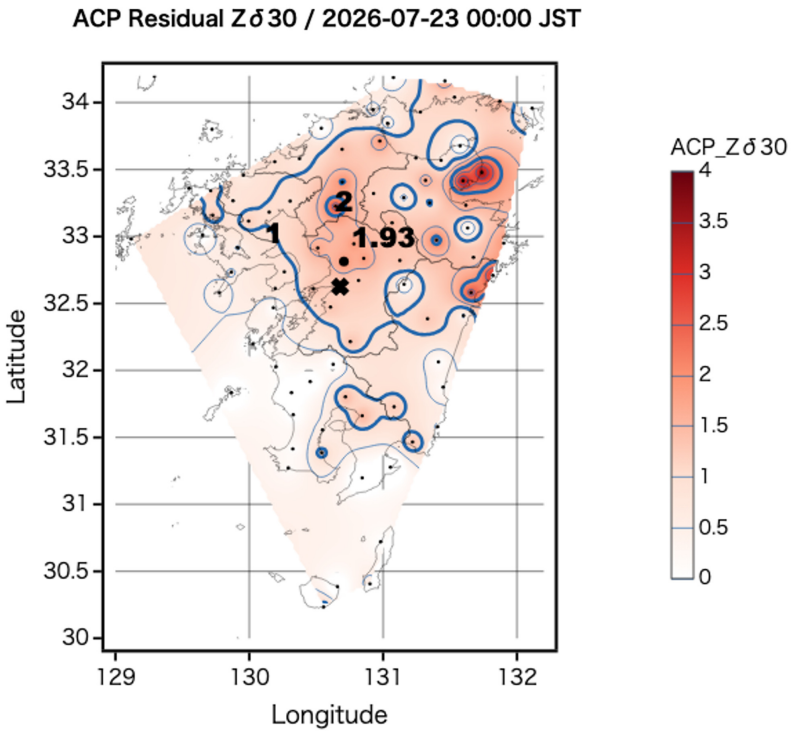


Figure 3(b). Contour map of the residual and normalized ACP values derived from multiple stations at 00:00 JST on 23 July. The numerals 1 and 2 indicate 1σ and 2σ, respectively. Small black dots denote AMeDAS stations, whereas the Kumamoto station shown in Fig. 3(a) is indicated by a slightly larger dot, with a residual ACP value of 1.93σ. Thus, the area extending from the Kumamoto station toward the northern peak exceeding 2σ is likely to exhibit enhanced ACP activity. Another region with even stronger ACP enhancement is also evident to the northeast of the EQ epicenter.

Figure 3(b) shows the residual ACP contour map over the Kyushu Island area at 00:00 JST on 23 July, four days before the EQ, because the period around midnight is considered particularly important when examining ACP variations. By making full use of the corresponding ACP values obtained at numerous AMeDAS stations, indicated by small black dots in the figure, as illustrated for the Kumamoto station in Fig. 3(a), we constructed the contour map shown in Fig. 3(b). The numerals 1 and 2 represent residual ACP values of 1σ and 2σ, respectively. The larger black dot indicates the Kumamoto station shown in Fig. 3(a), where the residual ACP value reaches 1.93σ. Therefore, the area extending from the Kumamoto station toward the northern peak exceeding 2σ may be regarded as a region of strongly enhanced ACP activity, located very close to the EQ epicenter indicated by a black cross. A further reddish

region, corresponding to the highest ACP values, is identified approximately 100 km northeast of the EQ epicenter. These ACP hotspots appear to be closely related to the distribution of the Kumamoto fault zones, which may be physically plausible in terms of possible radon emanation from active faults. Finally, this type of ACP contour mapping may provide useful information for constraining the possible location of an impending EQ.

4.3 VLF/LF Anomalies Indicative of the Perturbations in the Lower Ionosphere

The VLF/LF analysis algorithms of QIT have been established through successive revisions of data filtering procedures, dynamic nighttime windows, and related processing methods over the last half year, and can readily be applied to other propagation paths. Here, we apply our VLF analysis system to the propagation path from the JJI transmitter at Ebino, Miyazaki Prefecture, located about 60 km south of the EQ epicenter, as detected at the Osaka observing station. Fig. 4 illustrates the analysis results based on the nighttime fluctuation method Hayakawa (2025); Politis et al. (2024); Nanda et al. (2026), with particular attention to the behavior of the nighttime average amplitude shown in the top panel. The VLF/LF seismogenic anomaly is characterized by a depletion in nighttime amplitude prior to an EQ. The abscissa indicates the date in UT, while the ordinate represents the nighttime amplitude on each day normalized by its standard deviation calculated over the preceding 30 days. Thus, a definite anomaly is typically identified when the normalized amplitude decreases below -2.0σ. In Fig. 4, the nighttime signal amplitude starts to respond to seismic activity on 23 July, five days before the EQ, and one day before the EQ a conspicuous depletion below -2.0σ is observed. Although not shown in this paper, we also examined the corresponding VLF result at Chofu, which exhibited an anomaly on the same day with a smaller depletion of -1.6σ, providing additional support for the anomaly observed on the JJI–Osaka propagation path. However, the exact location of the possible lower-ionospheric perturbation cannot be determined from these observations alone. The simultaneous detection of anomalous decreases at Osaka and Chofu increases the reliability of the identified VLF propagation anomaly, although we can conclude only that the perturbation was located, at least, west of Osaka. On the other hand, the possible location of the impending EQ can be constrained using the AMeDAS analysis described in the previous subsection. The VLF finding for this EQ differs considerably from that reported for the 2016 EQ, for which the VLF perturbation was most strongly enhanced approximately 5–3 days before the EQ Asano and Hayakawa (2018), whereas for the 2026 EQ the strongest perturbation occurred immediately before the EQ.

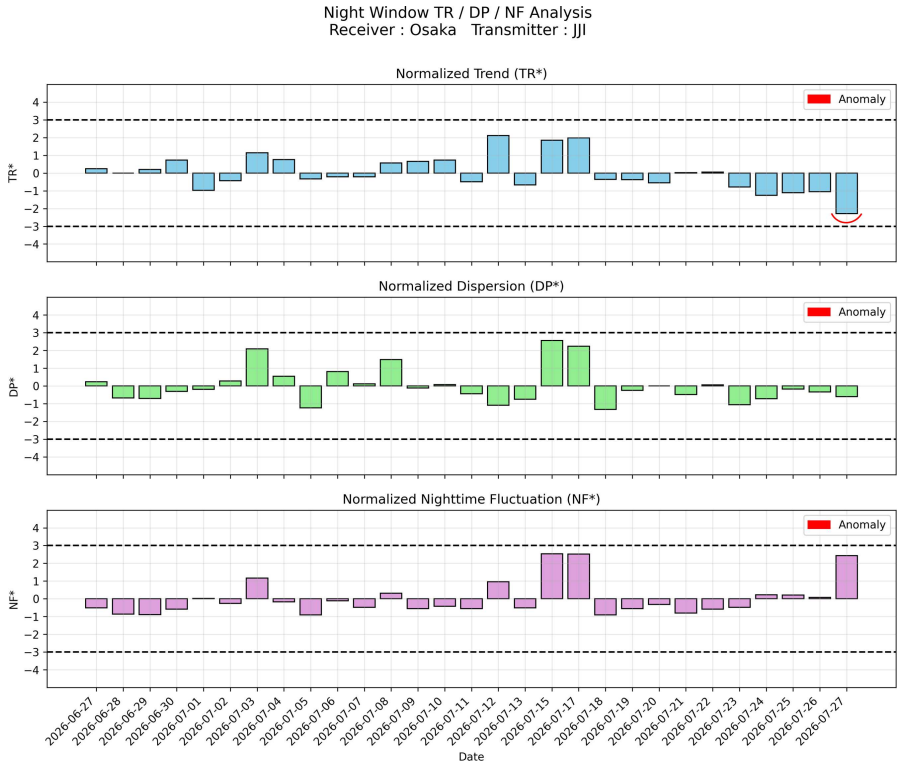


Fig. 5: Temporal evolution of the VLF analysis results for the JJI–Osaka propagation path based on the conventional nighttime fluctuation method. The top panel shows the average nighttime amplitude, normalized by the standard deviation (σ) calculated over the preceding 30 days, with the normalized values plotted on the ordinate. The second panel shows the nighttime fluctuation as another independent parameter, while the third panel represents the nighttime fluctuation as a dependent quantity derived from the two parameters shown above. The maximum anomaly, characterized by the strongest depletion, is observed one day before the EQ, when a conspicuous VLF anomaly is evident.

4.4 Ionospheric F Region Anomalies:

Figure 5(a) compares the temporal behavior at four vertical sounding stations: Wakkanai, Kokubunji, Yamagawa, and Okinawa. We plot $N_{\mathrm{m}}F2$ and $\Delta N_{\mathrm{m}}F2$ for each station, where red indicates an increase (positive deviation) and blue indicates a decrease (negative deviation) in $N_{\mathrm{m}}F2$. The bottom two panels are also shown again to facilitate a direct comparison with the solar–terrestrial conditions. Our primary target station is Yamagawa, located less than 100 km from the EQ epicenter; however, because the ionosphere is sensitive to various environmental factors, results from all four stations are presented for comparison. The figure suggests that the positive anomalies ($> 3\sigma$) observed at Wakkanai and Yamagawa on 24 July may be explained

as a positive ionospheric storm effect driven by geomagnetic activity. This tendency appears to be consistent with previous observations in the Japanese sector Liu et al. (2013). The interpretation that the positive deviations observed at all stations from 20 July to 2 August were associated with enhanced solar activity also appears reasonable. Finally, the oscillatory variations observed at Yamagawa from 12:00 JST on 26 July to 12:00 JST on 27 July, approximately 1.2–2.2 days before the EQ, are particularly interesting as a possible precursor, similar to the behavior reported for the 2024 Noto Peninsula EQ Yang et al. (2026).

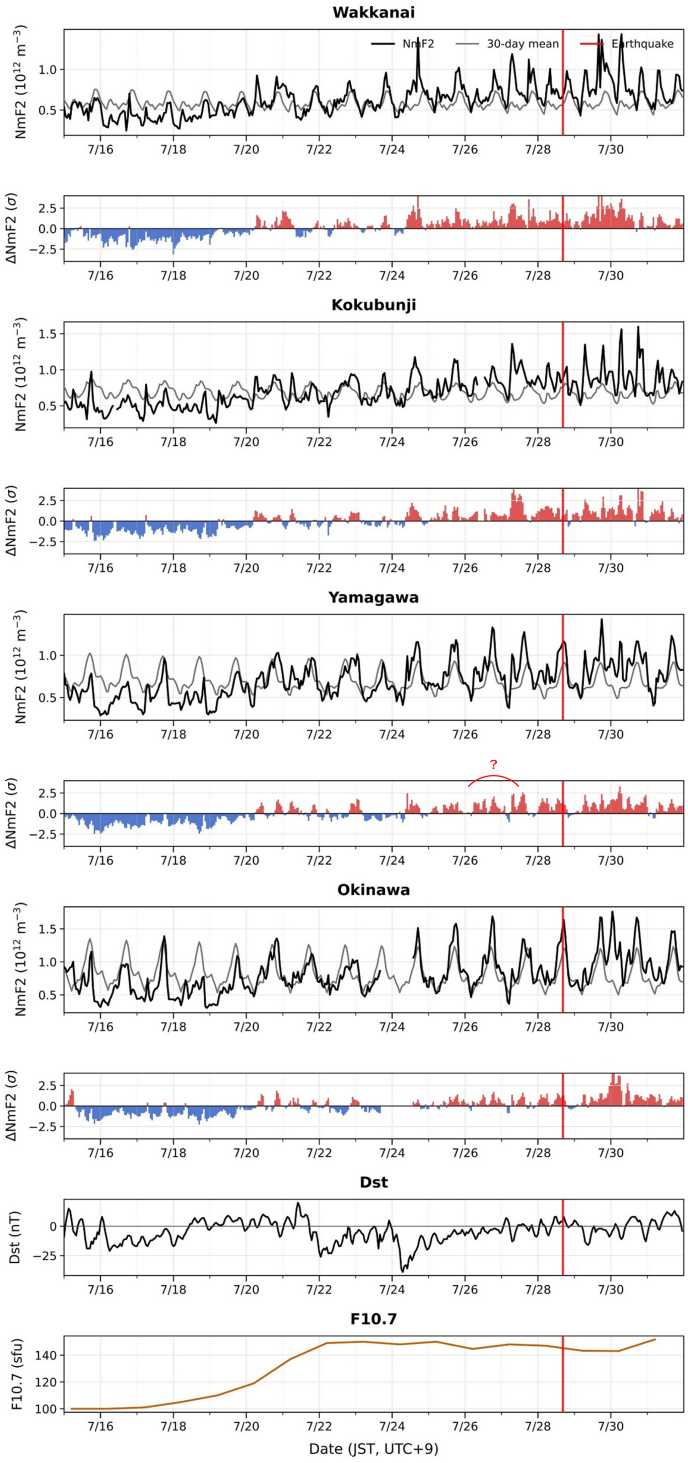


Figure 5(a). Temporal evolution of $N_{\mathrm{m}}F2$ and $\Delta N_{\mathrm{m}}F2$ at four Japanese vertical sounding stations: Wakkanai, Kokubunji, Yamagawa (the station closest to the EQ epicenter), and Okinawa. Red indicates an increase (positive deviation) in $N_{\mathrm{m}}F2$, whereas blue indicates a decrease (negative deviation). The bottom two panels show the temporal evolution of solar activity expressed by F10.7 and geomagnetic activity expressed by Dst (nT), respectively, for direct comparison with the ionospheric variations. The vertical red line indicates the occurrence time of the EQ.

To visualize this oscillatory behavior more clearly, Figure 5(b) presents the $N_{\mathrm{m}}F2$ wavelet spectra at the four stations from 24 July to 28 July. The middle and leftmost portions of the Kokubunji and Okinawa spectra, respectively, are blank because of missing data. The wavelet magnitude was normalized using the maximum $N_{\mathrm{m}}F2$ value at each station to facilitate comparison among the stations. Since solar radiation controls photochemical processes in the ionosphere and the mid-latitude ionosphere is also influenced by atmospheric semidiurnal tides, periodicities of approximately 24 h and 12 h are clearly evident at all stations, as shown in the figure. In addition, oscillatory variations with a period of approximately 6 h are clearly observed only at Yamagawa from 12:00 JST on 26 July to 12:00 JST on 27 July, corresponding to about 1–2 days before the EQ. Similar patterns are also visible, although less clearly, at Okinawa, Kokubunji, and Wakkanai. However, further analysis is required before drawing a definite conclusion regarding the possible seismogenic origin of these oscillations.

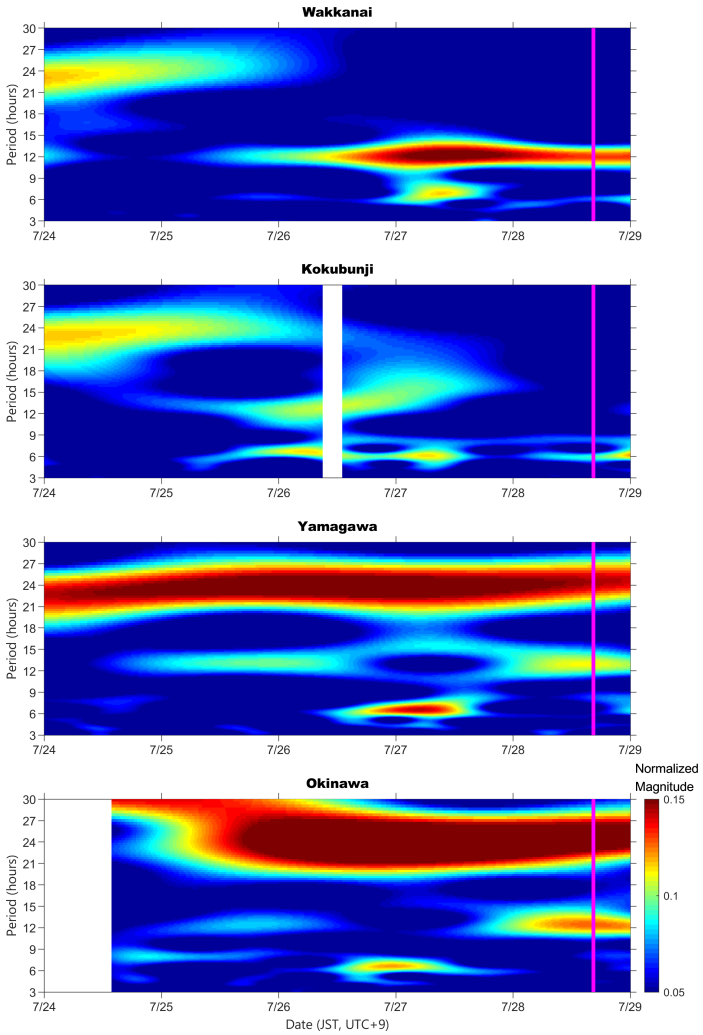


Figure 5(b). $N_{\mathrm{m}}F2$ wavelet spectra at the four stations from 24 July to 28 July. The middle and leftmost portions of the Kokubunji and Okinawa spectra, respectively, are blank due to missing data. The wavelet magnitude is normalized by the maximum $N_{\mathrm{m}}F2$ value at each station to facilitate comparison of the results among the stations. The vertical red line indicates the occurrence time of the EQ.

5 Satellite Observational Results:

In order to support the above ground-based observational results, we provide supplementary satellite observations of multiple parameters, including thermal parameters (T, RH, and ACP) Nanda et al. (2026), acoustic observations using an AGW proxy derived from ERA data Yang et al. (2019), electromagnetic observations of

GPS TEC obtained from GIM and GPS/IGS stations Pal et al. (2026), and mesosphere/thermosphere variability based on TIMED/SABER observations Phanikumar et al. (2018). Detailed explanations of the individual methodologies are not provided here, because they have already been described in the above-cited studies; therefore, only the corresponding observational results are presented.

5.1 Thermal parameters: T, RH, and ACP

The epicentral region was generally warmer than the surrounding area before the EQ. Figure 6 illustrates the daily variation in temperature differences associated with the Kumamoto EQ. The temperature difference increased from approximately 3 K on 23 July to a maximum of about 5 K on 26 July, two days before the EQ. From 27 July onward, the temperature difference progressively decreased toward 0 K, and almost no temperature difference remained after the event.

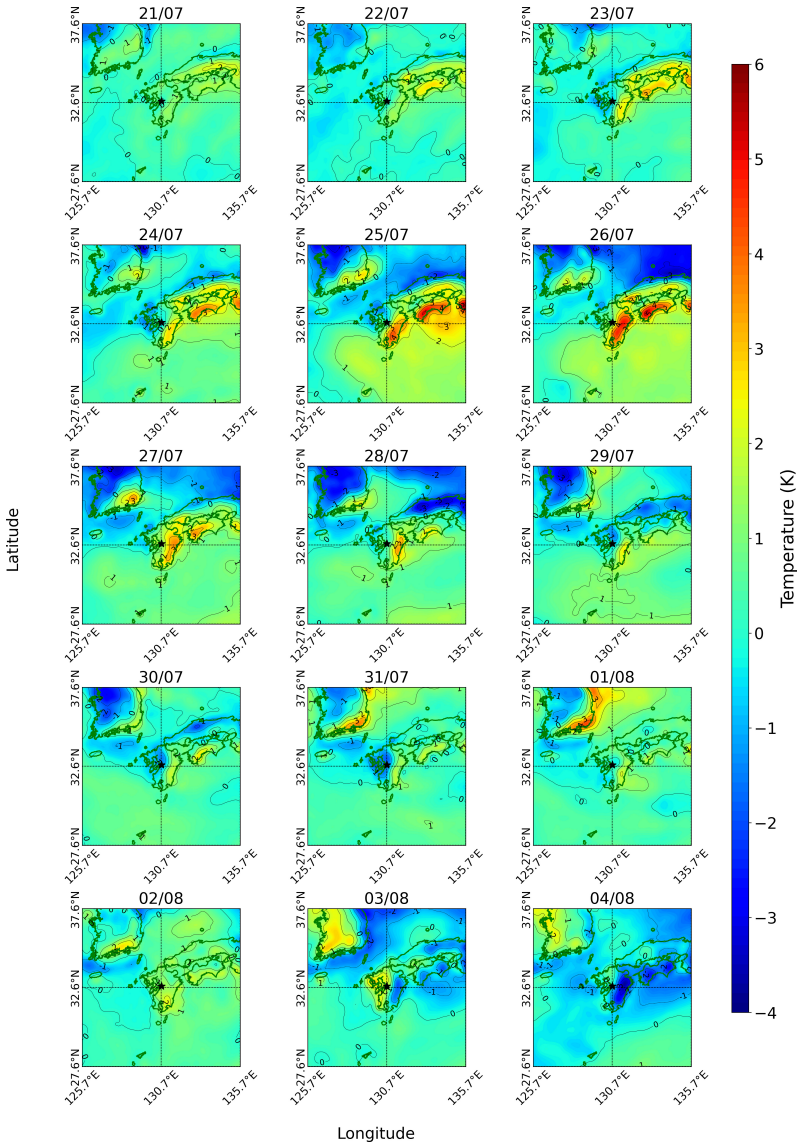


Figure 6. Daily variations of T during the Kumamoto EQ, with the center as the EQ epicenter. The EQ Day is 27 July.

Figure 7 shows the daily variations in relative humidity (RH) during the event. RH exhibited a pre-EQ enhancement of approximately 10–15%. On the day of the EQ, the RH difference decreased abruptly to nearly zero, and after the EQ, it became approximately 5% lower than the corresponding condition in the previous year.

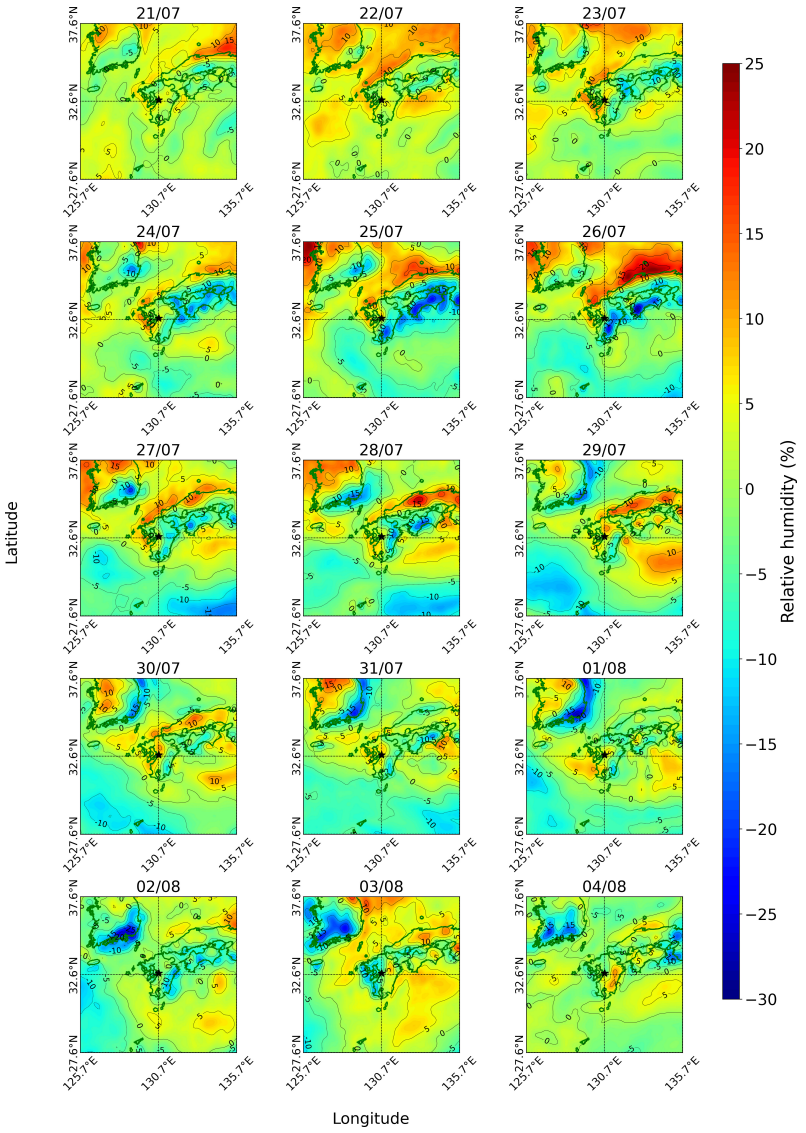


Figure 7. RH variations during the Kumamoto EQ with the center as the EQ epicenter.

Figure 8 illustrates the daily variations in ACP as a consequence of the changes shown in the previous two figures. The ACP difference increased to approximately 0.005 eV on 24 July and reached about 0.01 eV on 26 July, two days before the EQ. On the day of the EQ, the ACP difference returned to nearly 0 eV. During the post-event period, some days exhibited negative differences of approximately −0.005 eV.

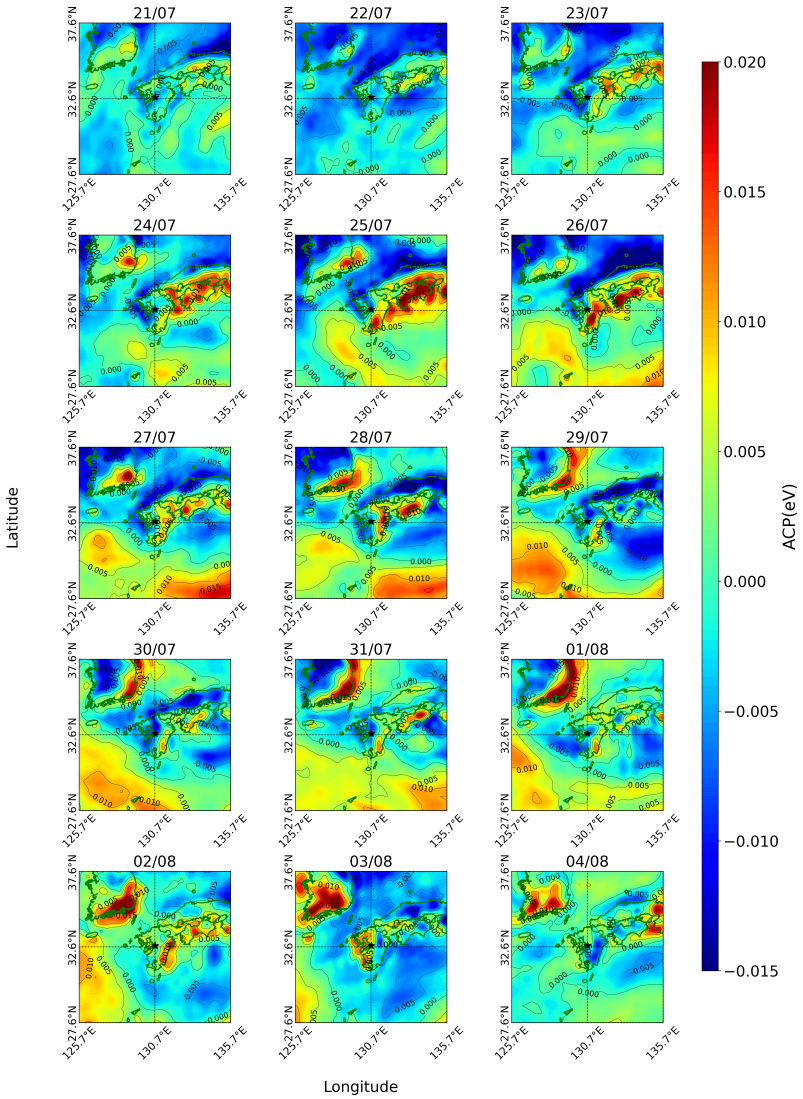


Figure 8.ACP variation during the Kumamoto EQ.

5.2 Acoustic Parameters: AGW

Focusing on the pre- and co-seismic interval, Figure 9(a) illustrates the ERA5-derived AGW potential energy (E_p) during the event, which shows a pronounced enhancement in the upper stratosphere–lower mesosphere several days before the 2026 Kumamoto EQ on 28 July. The strongest pre-seismic activity developed during 24–26 July, with E_p reaching approximately 18–24 J kg^{-1} near 45–47 km altitude. Toward the EQ day, the enhancement weakened, and E_p values around 28 July were comparatively lower, generally around 9–12 J kg^{-1} near 43–47 km. Thus, the most distinct AGW signature

was observed during the pre-seismic period, peaking approximately three days before the EQ, followed by a reduction toward the co-seismic time.

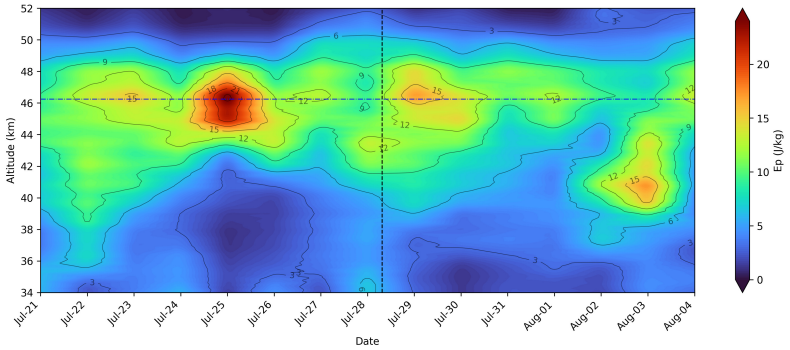


Figure 9(a). Daily variation of AGW activity during the event. The vertical line indicates the EQ occurrence time.

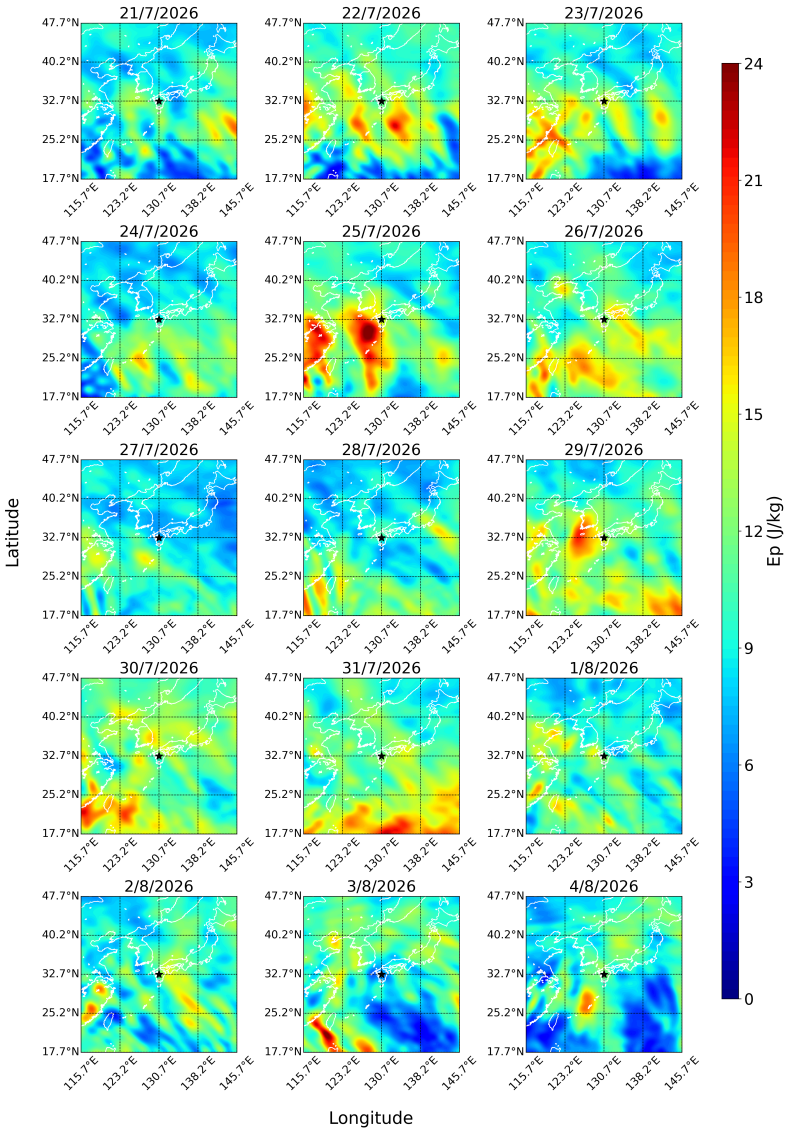


Figure 9(b). Daily variation of AGW activity during the event. The vertical line indicates the EQ occurrence time.

5.3 Electromagnetic parameters: GIM and GPS/IGS TEC

Figure 10(a) presents the temporal evolution of GPS-derived TEC anomalies at the GIM grid point located 9.13 km from the EQ epicenter. The anomaly amplitude increased progressively from about 4 TECU on DOY 202 (21 July) to a maximum of about 10 TECU on DOY 207 (26 July), two days before the EQ. On the day of

the event, the anomaly decreased to approximately 6 TECU. During the post-seismic period, TEC values again reached about 10 TECU on DOY 210 (29 July), and then gradually decreased to nearly 2 TECU by DOY 216 (4 August).

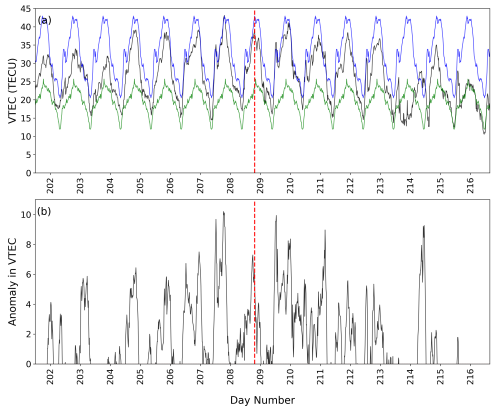


Figure 10(a). GPS VTEC variations as computed from the nearest grid point over the EQ epicenter, as observed from the GIM database. The vertical red lines indicate the EQ occurrence time.

The station-based TEC results shown in Fig. 10(b) exhibit a comparable but spatially variable response. At AIRA00JPN, located 95.83 km from the EQ epicenter, sustained TEC enhancements of approximately 3–8.5 TECU were observed during DOY 206–207 (25–26 July), with an anomaly of about 4 TECU on the EQ day. At GMSD00JPN, persistent anomalies of approximately 5.5–9.5 TECU occurred during DOY 207–208 (26–27 July), whereas no clear anomaly was detected on the day of the EQ. In the post-event interval, only isolated enhancements of around 4 TECU were observed. These results indicate that the ionospheric response was both temporally evolving and spatially nonuniform across the region.

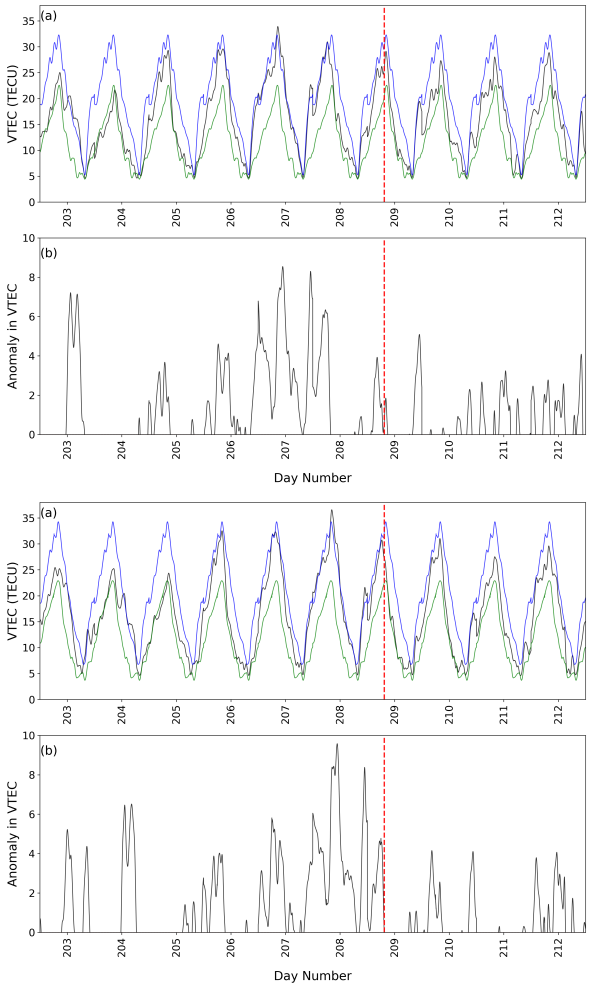
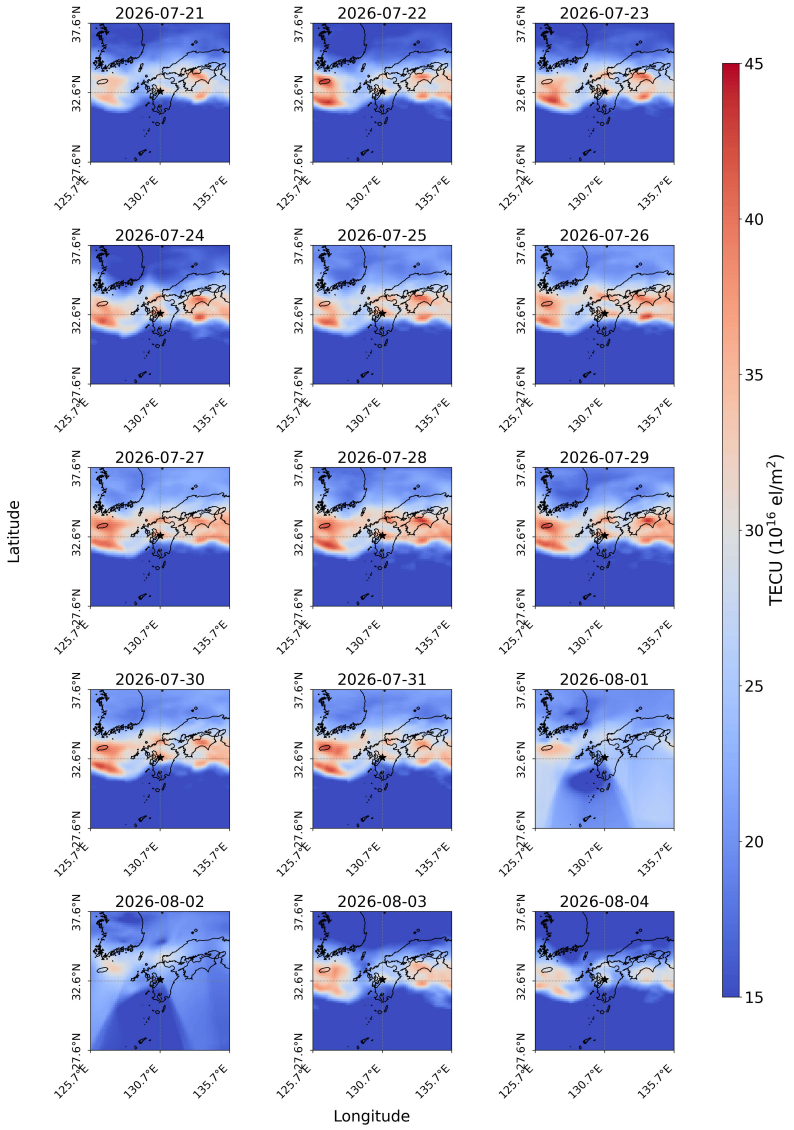


Figure 10(b). GPS VTEC variations for AIRA (Top) and GMSD (Bottom) IGS stations. The vertical red lines indicate the EQ occurrence.

Figure 10(c) illustrates the daily GIM VTEC distribution over the Kumamoto region from 21 July to 4 August 2026, with the EQ epicenter indicated in each panel. A persistent latitudinal gradient is evident, with relatively higher VTEC values in the northern part of the region and lower values toward the south. From 21 to 27 July, VTEC remains moderately enhanced, with localized maxima appearing near the EQ epicenter. On 28 July, a stronger enhancement is observed, which persists through 30–31 July. This enhancement is followed by a marked decrease on 1–2 August, after which a partial recovery occurs on 3–4 August. This sequence demonstrates pronounced pre-,

co-, and post-EQ ionospheric variability; however, any possible seismogenic contribution must be carefully distinguished from background geomagnetic and atmospheric influences.



captionsetuplabelformat=empty

Fig. 15: **Figure 10(c).** VTEC map as computed from the GIM database. A small red asterisk indicates the EQ epicenter.

5.4 Mesosphere/Thermosphere observations: SABER

Figure 11(a) shows the spatial distribution of TIMED/SABER observation points around the Kumamoto EQ region during 26–30 July 2026. The star marks the EQ epicenter near central Kyushu, while the colored points and short orbital segments indicate SABER measurements acquired on successive days. Several satellite passes occurred within a few degrees of the epicentral region, particularly on 29–30 July, providing useful coverage for examining possible mesospheric and lower-thermospheric perturbations associated with the EQ.

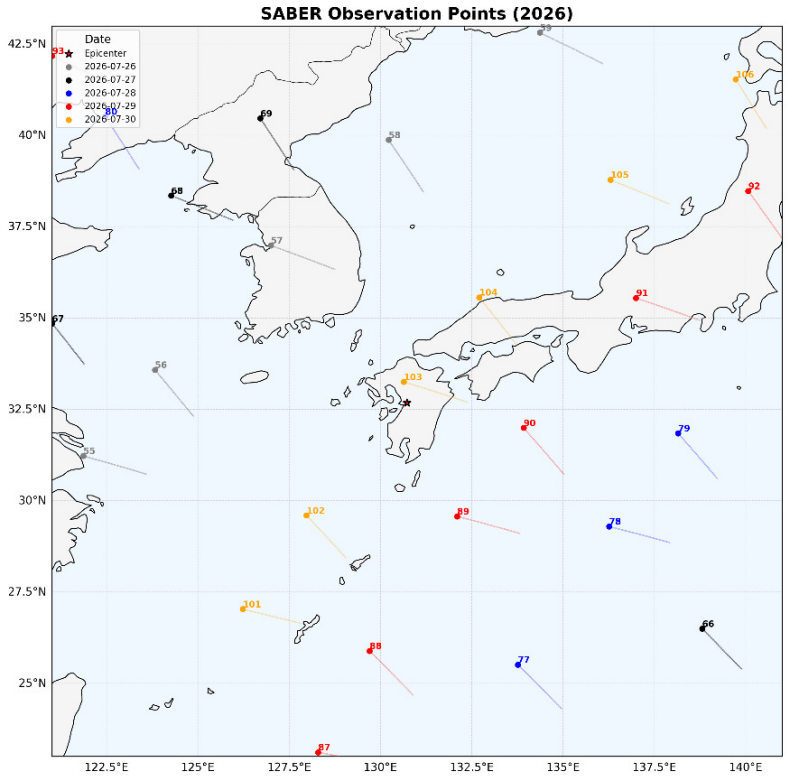


Figure 11(a). Spatial distribution of TIMED/SABER observation points around the epicenter of the 28 July 2026 Kumamoto EQ during the period 26–30 July 2026.

Figure 11(b) shows the TIMED/SABER-derived vertical profiles of nitric oxide (NO), ozone (O_3), OH emission rate, and temperature in the mesosphere–lower thermosphere before the EQ. Pronounced day-to-day variability is evident mainly within the ∼80–95 km altitude range. Nitric oxide exhibits an enhanced structure above ∼85 km, while ozone and OH show noticeable changes in both amplitude and vertical distribution, particularly between ∼83 and 92 km. The temperature profiles on 26–27 July also exhibit distinct vertical fluctuations, indicating a perturbed thermal

structure before the main shock. Overall, the SABER observations reveal appreciable pre-EQ variability in both the composition and thermal state of the upper atmosphere.

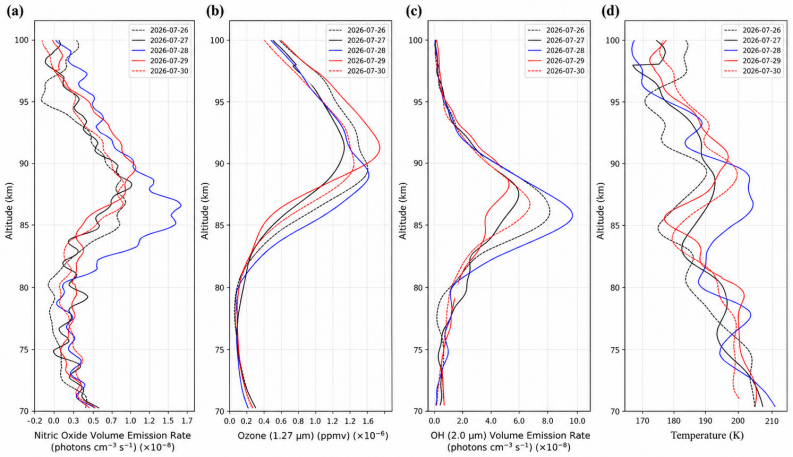


Figure 11(b). TIMED/SABER vertical profiles of nitric oxide (NO), ozone (O_3), OH emission rate, and temperature in the mesosphere–lower thermosphere.

5.5 Summary of Satellite Observations

Table 1 summarizes the results obtained from the satellite observations discussed in the previous subsections, with particular emphasis on the lead time of each observed anomaly relative to the EQ occurrence.

6 Discussion

A multi-parameter approach is essential for investigating possible EQ precursors because no single observable can reliably characterize the complex lithosphere–atmosphere–ionosphere coupling (LAIC) process De Santis et al. (2020); Hayakawa and Hobara (2024). By examining independent parameters across atmospheric and ionospheric layers, it becomes possible to assess whether anomalies exhibit consistent temporal and spatial behavior rather than occurring as isolated fluctuations. Such cross-validation provides a more robust basis for identifying potentially seismogenic disturbances. For practical short-term EQ precursory monitoring, ground-based observations have an important advantage because they generally provide higher temporal continuity and, in regional networks, finer spatial sampling than satellite measurements. In the present Kumamoto EQ event, ground-based observations showed several noteworthy changes during the days preceding the EQ. The meteorological parameters T, RH, and particularly ACP showed clear variations in the epicentral region, with the strongest spatial ACP enhancement near the Hinagu Fault and the EQ epicenter. This localization is potentially important because it suggests that meteorological parameters may provide not only temporal information on anomalous conditions but

Table 1: Summary of the key pre-EQ parameters and their lead times for the 2026 Kumamoto EQ.

Domain	**Parameter**	**Key pre-EQ value**	**Lead time**
Thermal	Temperature (T)	+5 K	2 days before the EQ
	Relative humidity (RH)	+10–15%	Before the EQ; exact maximum day not specified
	ACP	+0.01 eV	2 days before the EQ
Acoustic	AGW proxy	$\sim$ 18–24 J kg^{-1} at $\sim$ 45–47 km	2 days before the EQ
Electromagnetic	GIM TEC	10 TECU	2 days before the EQ
	GPS/IGS TEC	9.5 TECU (GMSD00JPN)	1 day before the EQ
Mesosphere/ Thermosphere	TIMED/SABER temperature	178 K at 84 km (minimum)	2 days before the EQ
	TIMED/SABER NO	No clear pre-EQ maximum	No clear pre-EQ effect
	TIMED/SABER O_3	1.2 units at 92 km (minimum)	1 day before the EQ
	TIMED/SABER OH	0.2 units at 83 km (minimum)	1 day before the EQ

also constraints on their spatial extent. A pronounced lower-ionospheric response was also detected along the JJI–Osaka VLF propagation path, with a weaker but contemporaneous anomaly observed at Chofu (Tokyo). The consistency between the two receiving stations strengthens the evidence for a disturbance affecting the JJI propagation region. In contrast, the F-region response derived from the Yamagawa ionosonde was less definitive, although short-period oscillatory variations were observed during the final 1–2 days before the EQ.

The satellite and reanalysis observations provide an independent view of the atmospheric and ionospheric environment during the same EQ period. A notable clustering of anomalies occurred approximately 1–2 days before the EQ: the epicentral region was about 5 K warmer than the reference condition, ACP increased by approximately 0.01 eV, and the GIM TEC anomaly reached about 10 TECU. GPS/IGS observations also showed enhanced regional TEC, reaching approximately 9.5 TECU at GMSD00JPN one day before the event. The close timing of the thermal, chemical-potential, and ionospheric responses is noteworthy, although temporal coincidence alone cannot establish a seismogenic origin, particularly because geomagnetic activity was variable during the analysis interval. The middle-atmospheric results provide additional information on the vertical structure of the disturbance. ERA5-derived gravity-wave potential energy showed a distinct pre-EQ enhancement during 24–26 July, reaching approximately 18–24 J kg^{-1} at 45–47 km altitude, with the strongest activity occurring about three days before the EQ and weakening toward the co-seismic

period. TIMED/SABER measurements similarly revealed appreciable pre-event variability in the mesosphere–lower thermosphere, mainly within 80–95 km, involving changes in temperature and in the vertical distributions of NO, O_3, and OH.

Taken together, the Kumamoto EQ observations indicate a temporally compact sequence of atmospheric and ionospheric disturbances during the final several days before the EQ. The most prominent features include localized lower-atmospheric T/RH/ACP anomalies, the pre-seismic AGW enhancement in the upper stratosphere–lower mesosphere, VLF propagation anomalies in the lower ionosphere, enhanced TEC in the F-region ionosphere, and compositional and thermal variability in the mesosphere–lower thermosphere. Rather than interpreting any individual parameter as an EQ precursor by itself, the scientific significance of this EQ event lies in the partial temporal and spatial coherence among independent observations at different altitudes. Such a multi-layer response provides a useful basis for examining possible LAIC pathways. Nevertheless, discrimination from ordinary meteorological variability, atmospheric-wave activity, and solar–geomagnetic disturbances remains essential, and the robustness of these signatures should ultimately be tested against non-EQ control periods and a larger population of seismic events.

7 Conclusion

We investigated possible precursory signatures associated with the recent 2026 Kumamoto EQ using a coordinated multi-parameter approach that combines ground- and satellite-based observations across different atmospheric and ionospheric regions. We placed greater emphasis on ground-based measurements because of their higher temporal continuity and regional spatial resolution. The meteorological parameters T, RH, and particularly ACP showed clear pre-event variations, with the spatial distribution of ACP providing extremely useful information on the localization of the anomalous region. At the same time, sub-ionospheric VLF observations revealed lower-ionospheric perturbations during the final 1–2 days before the EQ. The satellite measurements complemented these results by showing that several thermospheric and ionospheric disturbances also became prominent within approximately the same pre-EQ interval. The occurrence of anomalies over a relatively narrow time window, extending from the near-surface atmosphere to the lower and upper ionosphere, is therefore consistent with the possibility of a comparatively rapid LAIC response, such as the fast-coupling channel (i.e., direct coupling) discussed in Hayakawa and Hobara (2024), although this interpretation still requires further validation using additional events and control periods.

An important practical implication of this study is the suitability of these heterogeneous observations for integration into the QIT multi-parameter monitoring framework. By combining automated data acquisition, standardized analysis procedures, anomaly detection, cross-parameter comparison, and synchronized dashboard visualization, QIT provides a common platform for examining the temporal and spatial coherence of possible precursor signatures across different geo-layers. This integrated architecture is particularly important for moving from retrospective event analysis to prospective, continuous, and operational monitoring. A future comparison with the

stronger previous 2016 Kumamoto EQ sequence Schekotov et al. (2017) should help assess the reproducibility of the observed signatures and further clarify the physical characteristics of the LAIC process.

Acknowledgements. The authors gratefully acknowledge Gopi K. Seemala for providing GPS-TEC software, version 3.5, which was used for a substantial part of the TEC-related data processing and analysis. The authors also acknowledge the data services and scientific teams of NOAA, ECMWF, the International GNSS Service (IGS), Global Ionospheric Maps (GIM), and NASA OMNIWeb for providing the meteorological, atmospheric, ionospheric, and solar–terrestrial datasets used in this study. S. Sasmal acknowledges financial support from the Japan Trust International Research Cooperation Program under the National Institute of Information and Communications Technology (NICT) for overseas research activities.

Declarations

- Funding: This research received no external funding.
- Data availability: The open-source datasets used in this study are available from the following sources: U.S. Geological Survey (USGS) earthquake data (https://earthquake.usgs.gov/); NASA OMNIWeb solar and geomagnetic data (https://omniweb.gsfc.nasa.gov/); NOAA Physical Sciences Laboratory (PSL) NCEP/NCAR reanalysis data (https://psl.noaa.gov/data/gridded/data.ncep.reanalysis.html); ERA5 reanalysis data from the Copernicus Climate Data Store (https://cds.climate.copernicus.eu/); GNSS/GPS observation data from the International GNSS Service (IGS) (https://igs.bkg.bund.de/searchRINEX); and surface meteorological observations from the Automated Meteorological Data Acquisition System (AMeDAS) of the Japan Meteorological Agency (JMA) (https://www.jma.go.jp/). All websites were accessed during 1 August to 10 October October 2026.

References

Akhoondzadeh, M., De Santis, A., Marchetti, D., Piscini, A., Jin, S.: Anomalous seismo-LAI variations potentially associated with the 2017 Mw = 7.3 sarpol-e zahab (iran) earthquake from Swarm satellites, GPS-TEC and climatological data. Adv. Space Res. **64**, 143–158 (2019)

Asano, T., Hayakawa, M.: On the tempo-spatial evolution of the lower ionospheric perturbation for the 2016 kumamoto earthquakes from comparisons of VLF propagation data observed at multiple stations with wave-hop theoretical computations. Open J. Earthq. Res. (OJER) **7**, 161–185 (2018)

Blaunstein, N., Hayakawa, M.: Sinergy of Natural Phenomena in the Near-Earth Environment Via a Prism of the MaLAIM Coupling Mechanism, p. 138. GlobeEdit, London, UK (2026)

Conti, L., Picozza, P., Sotgiu, A.: A critical review of ground-based observations of earthquake precursors. Front. Earth Sci. **9**, 676766 (2021)

D'Arcangelo, S., Regi, M., De Santis, A., Perrone, L., Cianchini, G., Soldani, M., Piscini, A., Fidani, C., Sabbagh, D., Lepidi, S., *et al.*: A multiparametric-multilayer comparison of two geophysical events in the tonga-kermadec subduction zone: The 2019 M7.2 earthquake and 2022 hunga ha'apai eruption. Front. Earth Sci. **11**, 12677411 (2023)

De Santis, A., Cianchini, G., Marchetti, D., Piscini, A., Sabbagh, D., Perrone, L., Campuzano, S.A., Inan, S.: A multiparametric approach to study the preparation phase of the 2019 M7.1 ridgecrest (california, usa) earthquake. Front. Earth Sci. **8**, 540398 (2020)

De Santis, A., Cianchini, G., Perrone, L., Soldani, M., Rahimi, H., Alimoradi, H.: Foundation for an operational earthquake prediction system. Geosciences **15**, 69 (2025)

Draz, M.U., Shah, M., Jamjareegulgarn, P., Shahzed, R., Hasan, A.M., Ghamry, N.A.: Deep machine learning based possible atmospheric and ionospheric precursors of the 2021 Mw7.1 japan earthquake. Remote Sens. **15**, 1904 (2023)

Ghosh, S., Sasmal, S., Maity, S.K., Potirakis, S.M., Hayakawa, M.: Thermal anomalies observed during the crete earthquake on 27 september 2021. Geosciences **14**, 73 (2024)

Hayakawa, M.: Electromagnetic phenomena associated with earthquakes: A frontier in terrestrial electromagnetic noise environment. In: Pandalai, S.G. (ed.) Recent Research Developments in Geophysics, pp. 81–112. Research Signpost, Trivandrum, India (2004)

Hayakawa, M. (ed.): Electromagnetic Phenomena Associated with Earthquakes, p. 279. Transworld Research Network, Trivandrum, India (2009)

Hayakawa, M.: Earthquake Prediction with Radio Techniques, p. 294. John Wiley and Sons, Singapore (2015)

Hayakawa, M.: Review of subionospheric VLF/LF radio signals for the study of seismogenic lower ionospheric perturbations. Atmosphere **16**, 1312 (2025)

Hayakawa, M., Hobara, Y.: Integrated analysis of multi-parameter precursors to the fukushima offshore earthquake (Mj = 7.3) on 13 february 2021 and lithosphere–atmosphere–ionosphere coupling channels. Atmosphere **15**(8), 1015 (2024)

Hayakawa, M., Hirooka, S., Michimoto, K., Potirakis, S.M., Hobara, Y.: Meteorological anomalies during earthquake preparation: A case study of the 1995 kobe earthquake (M=7.3) based on statistical and machine leaning-based analyses. Atmosphere **16**,

88 (2025)

Hayakawa, M., Izutsu, J., Schekotov, A., Yang, S.S., Solovieva, M., Budilova, E.: Lithosphere-atmosphere-ionosphere coupling effects based on multiparameter precursor observations for february–march 2021 earthquakes (M 7) in the offshore of tohoku area of japan. Geosciences **11**, 481 (2021)

Hinata, H., Michimoto, K., Ozawa, Y., Hayakawa, M.: A study on lithosphere-atmosphere-ionosphere coupling channel for the 1995 kobe earthquake, by including ground-based meteoeorological anomalies. Open J. Earthq. Res. (OJER) **14**(2), 75–105 (2025)

Hayakawa, M., Potirakis, S.M., Hirooka, S., Hobara, Y.: Meteorological anomalies based on AMeDAS data for the 1995 kobe earthquake: Critical natura time analysis. Open J. Earthq. Res. (OJER) **14**(2), 67–84 (2025)

Hayakawa, M., Schekotov, A., Izutsu, J., Yang, S.S., Solovieva, M., Hobara, Y.: Multiparameter observation of seismogenic phenomena related to the tokyo earthquake (M=5.9) on 7 october 2021. Geosciences **12**, 265 (2022)

Haider, S.F., Shah, M., Li, B., Jamjareegulgarn, P., Oliveira-Junior, J., Zhou, C.: Synchronized and co-located ionospheric and atmospheric anomalies associated with the 2023 Mw7.8 turkey earthquake. Remote Sens. **16**, 222 (2024)

Liu, J.Y., Chen, C.H., Tsai, H.F.: A statistical study on seismo-ionospheric precursors of the total electron content associated with 146 M $\geq$ 6.0 earthquakes in japan during 1998–2011. In: Hayakawa, M. (ed.) Earthquake Prediction Studies: Seismo Electromagnetics, pp. 17–29. TERRAPUB, Tokyo, Japan (2013)

Liu, J., Zhang, X., Yang, X., Yang, M., Zhang, T., Bao, Z., Wu, W., Qiu, G., Yang, X., Lu, Q.: The analysis of lithosphere-atmosphere-ionosphere coupling associated with the 2022 luding Ms6.8 earthquake. Remote Sens. **15**, 4042 (2023)

Marchetti, D., De Santis, A., Shen, X., Campuzano, S.A., Perrone, L., Piscini, A., Giovambattista, R.D., Jin, S., Ippolito, A., Cianchini, G., *et al.*: Possible lithosphere-atmosphere-ionosphere coupling effects prior to the 2018 Mw = 7.5 indonesia earthquake from seismic, atmospheric and ionospheric data. J. Asian Earth Sci. **188**, 104097 (2020)

Molchanov, O., Fedorov, E., Schekotov, A., Gordeev, E., Chebrov, V., Surkov, V., Rozhnoi, A., Andreevsky, S., Iudin, D., Yunga, S., *et al.*: Lithosphere-atmosphere-ionosphere coupling as governing mechanism for preseismic short-term events in atmosphere and ionosphere. Nat. Hazards Earth Syst. Sci. **4**, 757–767 (2004)

Molchanov, O.A., Hayakawa, M.: Seismo Electromagnetics and Related Phenomena: History and Latest Results, p. 189. TERRAPUB, Tokyo, Japan (2008)

Marchetti, D., Zhu, K., Picsini, A., Ghamry, E., Shen, X., Yan, R., He, X., Wang, T., Chen, W., Wen, J., *et al.*: Changes in the lithosphere, atmosphere and ionosphere before and after the Mw = 7.7 jamaica 2020 earthquake. Remote Sens. Environ. **307**, 114146 (2024)

Marchetti, D., Zhu, K., Piscini, A., Ghamry, E., Shen, X., Yan, R., He, X., Wang, T., Chen, W., Wen, W., Wen, J., Zhang, Y., Cheng, Y., Fan, M., Zhang, D., Zhang, H., Venura, G.: Changes in the lithosphere, atmosphere, and ionosphere before and during the Mw=7.7 jamaica 2020 earthquake. Remote Sens. **307**, 114146 (2024)

Nanda, K., Brawar, B., Hayakawa, M., Hobara, Y., Potirakis, S.M., Maurya, A.K., Pandey, U., Datta, A., Sasmal, S.: A multi-parametric investigation of seismogenic signals: A case study of the 2018 aomori earthquake (Mw 6.2). Open J. Earthq. Res. (OJER) **15**(2), 11–38 (2026)

Ouzounov, D., Pulinets, S., Davidenko, D., Rozhnoi, A., Solovieva, M., Fedun, V., Dwivedi, B.N., Rybin, A., Kafatos, M., Taylor, P.: Transient effects in atmosphere and ionosphere preceding the 2015 M7.8 and M7.3 gorkha–nepal earthquakes. Front. Earth Sci. **9**, 757358 (2021)

Ouzounov, D., Pulinets, S., Hattori, K., Taylor, P. (eds.): Pre-Earthquake Processes: A Multidisciplinary Approach to Earthquake Prediction Studies. AGU Geophysical Monograph, vol. 234, p. 365. Wiley, New York, NY, USA (2018)

Pulinets, S.A., Boyarchuk, K.: Ionospheric Precursors of Earthquakes, p. 315. Springer, Berlin/Heidelberg, Germany (2004)

Picozza, P., Conti, L., Sotigiu, A.: Looking for earthquake precursors from space: A critical review. Front. Earth Sci. **9**, 6767775 (2021)

Parrot, M., Li, M.: Statistical analysis of the ionospheric density recorded by the DEMETER satellite during seismic activity. In: Ouzounov, D., Pulinets, S., Hattori, K., Taylor, P. (eds.) Pre-Earthquake Processes: A Multidisciplinary Approach to Earthquake Prediction Studies. AGU Geophysical Monograph, vol. 234. Wiley, New York, NY, USA (2018). Chap. 18

Phanikumar, D.V., Maurya, A.K., Kumar, K.N., Venkatesham, K., Singh, R., Sharma, S., Naja, M.: Anomalous variations of VLF subionospheric signal and mesospheric ozone prior to 2015 gorkha nepal earthquake. Scientific Reports **8**, 9381 (2018)

Pal, S.K., Nanda, K., Sarkar, S., Potirakis, S.M., Hayakawa, M., Sasmal, S.: Comparative statistical detection of ionospheric GPS-TEC anomalies associated with the 2021 haiti and 2022 cyprus earthquakes. Geosciences **16**, 3 (2026)

Pulinets, S., Ouzounov, D.: Lithosphere-atmosphere-ionosphere coupling (LAIC) model—a unified concept for earthquake precursors validation. J. Asian Earth Sci. **41**, 371–382 (2011)

Pulinets, S.A., Ouzounov, D., Karelin, A., Boyarchuk, K.: Earthquake Precursors in the Atmosphere and Ionosphere: New Concepts, p. 294. Springer, Dordrecht, The Netherlands (2020)

Politis, D.Z., Potirakis, S.M., Contoyiannis, Y.F., Potamitis, I., Sasmal, S., Yang, S.S., Hayakawa, M.: Lower-ionosphere anomalies prior to strong earthquakes that occurred in north-central mainland greece on march 2021 as revealed by multi-method analysis of VLF sub-ionospheric propagation data. Ann. Geophysics **66**(6), 645 (2024)

Politis, D.Z., Sasmal, S., Hayakawa, M., Haralambous, H., Datta, A., Potirakis, S.M.: A six-year (2014–2020) statistical correlation study of VLF terminator time shift with earthquakes in japan. Remote Sens. **16**, 4162 (2024)

Parrot, M., Tramutoli, V., Liu, J.Y., Pulinets, S., Ouzounov, D., Genzaro, N., Lisi, M., Hattori, K., Namgaladze, A.: Atmospheric and ionospheric coupling phenomena associated with large earthquakes. Eur. Phys. J. Spec. Topics **230**, 197–225 (2021)

Rodger, C.J., Cliverd, M.A.: Modelling of sub-ionospheric VLF signal perturbations associated with earthquakes. Radio Sci. **34**(5), 1177–1185 (1999)

Sorokin, V.V., Chmyrev, V., Hayakawa, M.: Electrodynamic Coupling of Lithosphere-Atmosphere-Ionosphere of the Earth, p. 355. NOVA Science Pub. Inc., New York, NY, USA (2015)

Sasmal, S., Chowdhury, S., Kundu, S., Politis, D.Z., Potirakis, S.M., Balasis, G., Hayakawa, M., Chakrabarti, S.K.: Pre-seismic irregularities during the 2020 samos (greece) earthquake (M = 6.9) as investigated from multi-parameter approach by ground and space-based techniques. Atmosphere **12**, 1059 (2021)

Sasmal, S., Chowdhury, S., Kundu, S., Ghosh, S., Politis, A.Z., Potirakis, S.M., Hayakawa, M.: Multi-parametric study of seismogenic anomalies during the 2021 crete earthquake (M=6.0). Ann. Geophysics **66**(6), 646 (2024)

Schekotov, A., Izutsu, J., Asano, T., Potirakis, S.M., Hayakawa, M.: Electromagnetic precursors to the 2016 kumamoto earthquakes. Open J. Eathq. Res. (OJER) **6**, 168–179 (2017)

Sasmal, S., Nanda, K., Hayakawa, M., Solovieva, M., Kopylova, G., Potirakis, S.M.: Towards understanding earthquake preparatory dynamics: A multi-parametric investigation of the 2025 kamchatka Mw 8.8 event. Atmosphere **16**, 1328 (2025)

Shah, M., Shazad, R., Jamjareegulgarn, P., Ghaffar, B., Olveira-Junior, J., Hassan, A.M., Ghamry, N.A.: Machine-learning-based lithosphere-atmosphere-ionosphere coupling associated with Mw $>$ 6 earthquakes in america. Atmosphere **14**, 1236 (2023)

Tronin, A.A., Hayakawa, M., Molchanov, O.A.: Thermal IR satellite data application for earthquake research in japan and china. J. Geodyn. **33**, 477–487 (2002)

Tronin, A.: Atmosphere-lithosphere coupling. thermal anomalies on the earth surface in seismic process. In: Hayakawa, M., Molchanov, O.A. (eds.) Seismo Electromagnetics: Lithosphere-Atmosphere-Ionosphere Coupling, pp. 173–176. TERRAPUB Co., ??? (2002)

Yang, S.S., Asano, T., Hayakawa, M.: Abnormal gravity wave activity in the stratosphere prior to the 2016 kumamoto earthquakes. J. Geophys. Res.: Space Physics **124**(2), 1410–1425 (2019)

Yang, S.S., Hobara, Y., Sasmal, S., Potirakis, S.M., Hayakawa, M.: Anomalies on ionospheric electron density before the 2024 noto peninsula earthquake using oblique ionosondes. Atmosphere **17**(7), 67 (2026)

Zhang, X., Liu, J., De Santis, A., Perrone, L., Xiong, P., Zhang, X.: Lithosphere-atmosphere-ionosphere coupling associated with four yutian earthquakes in china from GPS TEC and electromagnetic observations onboard satellites. J. Geodyn. **155**, 101943 (2023)